Eur. Phys. J. D **29**, 217–229 (2004)
DOI: 10.1140/epjd/e2004-00033-3

THE EUROPEAN PHYSICAL JOURNAL D

# Dynamics in a cluster under the influence of intense femtosecond hard X-ray pulses

Z. Jurek[a], G. Faigel, and M. Tegze

Research Institute for Solid State Physics and Optics, POB 49, 1525 Budapest, Hungary

Received 22 September 2003
Published online 9 March 2004 – 

**Abstract.** In this paper we examine the behavior of small cluster of atoms in a short (10–50 fs) very intense hard X-ray (10 keV) pulse. We use numerical modeling based on the non-relativistic classical equation of motion. Quantum processes are taken into account by the respective cross-sections. We show that there is a Coulomb explosion, which has a different dynamics than one finds in classical laser driven cluster explosions. We discuss the consequences of our results to single molecule imaging by the free electron laser pulses.

**PACS.** 61.80.-x Physical radiation effects, radiation damage – 36.40.-c Atomic and molecular clusters – 61.46.+w Nanoscale materials: clusters, nanoparticles, nanotubes, and nanocrystals

## 1 Introduction

Recently, there is a growing interest in the interaction of high intensity electromagnetic field with solids and small clusters of atoms. This interest is driven by two sources: (i) by the availability of short-pulse high-power laser sources in the few hundred nm wavelength range, and (ii) by the fact that the building of linac-based free-electron laser type hard X-ray sources became a reality [1,2]. In the case of the long wavelength laser radiation the interest shifted from the bulk-field to the cluster-field interaction. The cause of this is that the behavior of clusters under the influence of intense laser field shows several peculiarities. First, there is a photo induced Coulomb explosion [3]. Second, the interaction is much more energetic than that of isolated atoms [4,5]. Third, highly ionized states of the atoms appear [4]. Fourth, lately it was shown that even laser driven nuclear fusion could take place in small clusters of deuterium atoms [6]. This could eventually lead to the development of tabletop neutron sources.

On the other hand, short-pulsed intense hard X-ray sources also promise unique applications: the high energy of these photons allows time dependent spectroscopic investigations of deep atomic levels, the short wavelength makes possible structural investigations with atomic resolution on a time scale of 100 fs. So we can follow chemical reactions and biological processes in time. One can even think of imaging individual molecules, viruses or clusters of atoms and molecules using the very intense and short pulses of these X-ray sources [7]. Further, we could study exotic states of matter such as warm dense matter, etc. [8,9]. The treatment of the high-energy case requires a very different approach than the low photon energies. The reason is twofold: practical and theoretical. From the practical point of view the production of an intense hard X-ray photon beam requires many km long facility, which costs hundreds of millions of dollars, while a high power infrared laser source can be realized in normal laboratory environment for less then a million dollar. This difference results in a very different research strategy. While in the long wavelength case theory and experiments develop parallel, in the X-ray case no experiment can be done presently. However, there is a strong need for model calculations, which can predict the behavior of different forms of matter under the influence of intense X-ray beam. This information is necessary, because planning these large machines and working out the scientific case, one has to know how the optical elements and the sample will behave in the beam. Based on this we can plan future experiments and determine what kind of information can be gained from them.

This leads to the theoretical side. It is clear that in the X-ray case, the high energy of a single photon allows direct interaction with core electrons, so the ionization mechanism significantly differs from that of the low energy laser photons. This requires a different theoretical approach. We expect that quantum mechanics and quantum electrodynamics should be more often invoked than in the low energy case.

At the same time we know that the exact quantum treatment of a thousand particle system in intense electromagnetic field is out of the reach of present day computer capabilities. Therefore one has to find a border where quantum and classical description meet, meanwhile the

[a] e-mail: jurek@szfki.hu

behavior of the model system is not distorted significantly. The first steps in this direction have been done. There have been model calculations, which statistically describe a system after a single primary ionization event [10,11].

In this paper we describe a model calculation for the dynamics of atoms, ions, and electrons in a cluster, during an intense hard X-ray pulse. In this case many consecutive ionization (energy deposition) events in the system drive the cluster to highly ionized states, leading to Coulomb explosion. In the calculations we work with classical particles solving the classical equation of motion. The quantum mechanics and the quantum electrodynamics are included through cross-sections. In practice it means that the various events are taken into account by different probabilities. The motivation of these calculations comes from two sources: in one hand we would like to see the difference in the Coulomb explosions caused by low and high-energy photons. Secondly, we would like to examine, how realistic the single particle imaging by high intensity fs X-ray pulses is. In this article we concentrate on the Coulomb explosion and give only a brief comment on single particle imaging. The reason for this is that the imaging problem is very complex, it requires not only the knowledge of the dynamics of the cluster, but also the calculation of the intensity distribution of elastic and inelastic X-ray scattering and the reconstruction of atomic order from the scattering pattern. These questions will be addressed in forthcoming papers.

## 2 Model

In order to do a realistic modeling we have to use input parameters typical for the future linac based X-ray sources. Therefore, we give the relevant characteristics of these sources below: the pulse shape is Gaussian with full widths at half maximum $FWHM = 10$ and 50 fs; the number of photons/pulse is $N_{ph} = 5\times10^{12}$; the diameter of the probe beam at the sample is $d = 100$ nm (by focusing); the energy of the beam is $E = 10$ keV and it is linearly polarized. Before we continue with the description of our model, we would like to introduce a terminology: we will call a single X-ray pulse and all the events in the cluster from the start of the pulse to the end of it an "experiment".

Since our aim is the determination of the charge distribution in space and time, we follow every individual particle (atoms, ions, and electrons). This means the numerical solution of the classical equation of motion for all particles. Quantum mechanics is included via cross-sections, and taking into account discrete atomic energy levels in the ionization process. Here we would like to call the attention to a difference between calculations in the low and high-energy case. In the low energy case the laser field acts on the particles in two ways: it can strip weakly bound electrons by multiphoton process or optical tunneling, and it accelerates the ions and electrons as a classical field. The charged particles move large distances (compared to the cluster size) during half period of the field, which can be taken as homogeneous within the cluster, since the wavelength is much larger than the cluster size. In the X-ray case, the field is changing very fast both in time and space, so that there is no time for a particle to gain appreciable velocity and to move large distance [12] during half period of the incident beam. Therefore the X-ray field as a classical field can be neglected in the equation of motions. So the most important interaction, which alters the motion of charged particles, is the Coulomb interaction. This is taken into account in our calculations and the Coulomb interaction is not cut at any distance. However, close to the nuclei the Coulomb potential is regularized for two reasons: we know that in the vicinity of the nuclei the atomic electrons modify the pure Coulomb potential. Secondly, in the classical picture an electron could go very close to the positive nucleus and in this case the potential diverges to infinity, which cannot be handled numerically. Therefore in practice we use the following formula for the Coulomb interaction: $U(r) = q/\sqrt{r^2 + r_0^2}$, where $r_0$ was chosen in a way, not to violate the energy conservation within the numerical error [13].

The next approximation, which we have to mention, is the non-relativistic approach. This is justified by the low maximum velocity of electrons, which can be estimated from the incident photon energy and the binding energy of the electrons. Taking the parameters of the incident beam, the upper limit for electron energy is 10 keV. This corresponds to a velocity of about (1/5)th of the velocity of light. Therefore the non-relativistic treatment is justified.

At last we would like to specify the cross-sections. Analyzing the possible scattering processes we arrive at two types of cross-sections: photon-particle and particle-particle. In the former we include photon-electron, photon-atom, and photon-ion cross-sections. Photons with free electrons interact via Compton scattering. The differential and total cross-sections for this process are given in quantum electrodynamics handbooks [14]. Using the total Compton cross-section and the parameters of our experiment we can estimate the number of Compton scattered photons during the full length of the X-ray pulse. We get about 200 Compton scattering events in a 1500 atom system. This low number means that Compton scattering does not alter the time evolution of the charge distribution at a detectable level. Therefore we neglect it in the calculations. In the case of strongly bound electrons the dominating process is the photo effect. This is true for atoms and also for ions provided that they have electrons left on deep core levels. Photo effect cross-section data for ions were extrapolated from the atomic values [14]. Two approximations were used: first, we neglected the change of the wave function of the atomic electrons on removing electrons from the atom. Second, the probability of the photo effect was normalized to one electron (at a given state), and depending on the ionization state it was scaled by the number of electrons actually present on the ion at the state under consideration. The last possibility for the photon-atom interaction is the fluorescent process. In our case (low $Z$ sample) the probability of the fluorescent decay is low compared to the Auger process [15].

Considering the particle-particle type interactions, we can list atom-atom, atom-ion, ion-ion, electron-atom, electron-ion, and electron-electron interactions. We do not use explicitly cross-sections for atom-atom and atom-ion collisions. The reason is that these collisions come into play only at the very beginning of the X-ray pulse, since atoms are very rapidly ionized at the rising edge of the pulse and between ions the Coulomb interaction dominates. For those few atoms, which are not ionized the van der Waals type interaction which we use to mimic chemical bonding describes well enough the atom-atom and atom-ion collisions.

Ion-ion and electron-electron interactions are taken into account directly by the Coulomb interaction. Although this way quantum effects (like exchange interaction) are neglected, we expect that at the given experimental conditions (energy, density etc.), their contribution is minor.

The remaining two interactions, electron-atom and electron-ion are the most important ones. We can distinguish three types: the Auger process, the elastic scattering of electrons, and the secondary (often called impact) ionization by electrons. In the Auger process an electron from a higher level drops into a K hole (created previously in the photo effect), meanwhile an other electron from the higher level is emitted taking the excess energy. The lifetime for this process was taken from [16]. Probabilities were scaled similarly to the photo effect, using the values given for the basic Auger process.

The next interaction is the elastic scattering of electrons on atoms and ions. This does not play an important role in the time evolution of charge distribution. The reason is that this process does not change the number of charges, only the direction of their velocity. We checked the validity of the above statement by carrying out calculations with different elastic cross-sections. We tried both isotropic and non-isotropic cross-sections [17] and we did calculations without electron-atom elastic scattering. We found that there was no significant difference in the time dependence of the charge distributions among the three types of calculations. Therefore we switched off atom-electron elastic scattering. We have to mention, that part of the elastic scattering, namely the electron-ion interaction is taken into account anyway by the Coulomb interaction, which is present for all charged particles in the system.

In the secondary ionization an electron with high enough energy interacts with an atom or ion kicking out an electron from a bound state, meanwhile its kinetic energy decreases (so in this process the number of charges changes). It is clear from the literature that with the decrease of the energy the cross-section of this process increases. However, at very low energies (below 80 eV) this tendency changes, and the incident electron energy dependence of the cross-section shows a rapid decrease (Fig. 1). All in all in the lowest 80 eV region the description of the cross-section of the secondary ionization by electrons is problematic. Beside the atomic properties the details depend strongly on the chemical bonding and geometrical arrangement of atoms. Since in this region the cross-section values derived from different theoretical approaches [18–21] differ significantly and experimental data are scarce we tried two approaches with 50 and 80 eV turning points for a 1500 atom cluster and 50 fs pulse width. We found small differences in the cluster dynamics. These appeared close to the end of the X-ray pulse. The changes was so small that they do not effect the conclusions we draw from the calculations. Therefore in all the other calculations we used the 50 eV turning point curve for the cross-section of the secondary electron ionization.

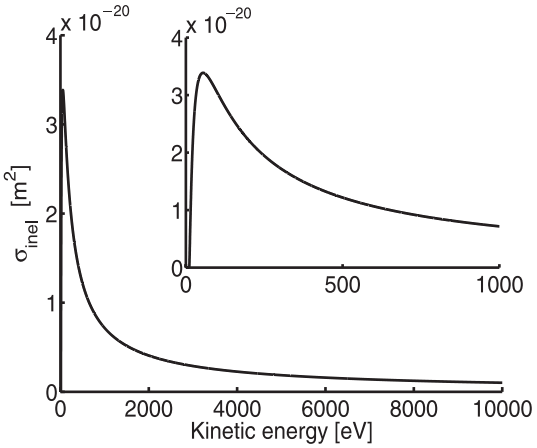


**Fig. 1.** Cross-section of electron impact ionization vs. incoming electron energy for neutral carbon atoms. The inset shows the cross-section enlarged in the low energy regime. Note that for ions the cross-section is different according to equation (1). The mean free path dynamically changes because of the inhomogen time-dependent atom-density.

In what follows we describe the mechanism of the modeling. The calculation proceeds via time steps. The typical value of a step is $10^{-3}$ fs. In every time steps two actions are done:

(i) Monte Carlo (M.C.);
(ii) solving the equation of motion.

In the M.C. sub-step we examine for all particles if any process (taken into account by cross-sections) happened or not. Therefore the probabilities of the photo effect and Auger process are normalized to one time step. For every atom and ion random numbers are generated to decide if these processes had taken place. The secondary ionization is calculated in a different way. First, the near neighbor atoms and the relative atom-electron velocities are determined for every electron. We attach to the electron a circular plate perpendicular to its velocity. The area of this plate is equal to the cross-section. This plate moves together with the electron sweeping a cylindrical volume. If in this volume there is an atom having bound electrons with low enough energy to kick out, a secondary ionization does happen.

At this point it is appropriate to discuss a delicate question: how we create a new particle in our classical model. This is the point where the classical and quantum picture have to be smoothly joined. It is clear from the above description of the model that electrons appear in the case of photo effect, Auger process, and secondary ionization. Let us start with the simplest case of the photo effect. This seems straightforward, since a photon comes in, and it looses all of its energy, which is given to one atomic electron. This simple picture is true if we look at the initial state as an atom at the origin and a photon at infinite and the final state as an ion in the origin and a kicked out electron at the infinite. However, in our calculations we follow the path of every particle, and we know that the stripped electron continuously moves out from the atom under consideration. On its path it interacts with other atoms, ions, and electrons present in the sample. Therefore we have to place the electron somewhere close to its parent atom and not at infinite. This raises two questions: where and with what velocity to put this electron. We use different values for K and L electrons. These values can be directly calculated using two plausible assumptions: (i) the distance and the magnitude of the velocity are fixed for a given shell independently of the ionization state of the atom; (ii) conservation of energy is satisfied. This way we arrive to distances about the Bohr radius, which is a natural border of the atom in the classical picture. The velocity cannot be simply $v = \sqrt{2E_{photon}/m_{el} - 2E_{binding}/m_{el}}$ because the electron should have this velocity at infinite distance from the ion. If we put the electron close to its parent atom, which is now a positive ion, the electron would slow down going to infinity. Therefore we have to give the electron a larger velocity to compensate this slowing down. If we want to be more precise, we have to take into account the field caused by all other charged particles (though in practice the leading term is the Coulomb potential of the closest ion). The last problem is the direction of the electron's velocity. The angular dependence of the cross-section of the photo effect is given in handbooks [14] for a linearly polarized incident photon. Therefore we use random directions with a distribution corresponding to the theoretical cross-section. The direction of the velocity fixes the position of the exact placement, since we put the electron in a way that it moves out radially from the atom. At last we have to mention that the energy and momentum conservations are satisfied in this process, so the ion takes recoil energy. For placing the electron in the Auger process, a similar mechanism is used. However, in the case of secondary ionization there is a significant difference. The cause is that here we have a three body problem. In this case we have an electron and an atom (or ion) in the initial state and two electrons and an ion in the final state. Placing the electrons with the proper velocities is not straightforward. The first problem is that there is no reliable data for the angular dependence of the cross-section of inelastic electron scattering. The simplest assumption is an isotropic emission of the secondary electrons and we use this in the calculations. To see the effect of non-isotropic emission we did model calculations with an angular distribution derived from quantum mechanical calculations [17]. There was a small change in the time evolution of the system. So our assumption of isotropic emission was justified. For the energy dependence of the cross-section we use a parameterized formula [22]:

$$\sigma_{inel} = \frac{S}{t + (u+1)/n} \left[ \frac{Q \ln t}{2} \left( 1 - \frac{1}{t^2} \right) + (2 - Q) \left( 1 - \frac{1}{t} - \frac{\ln t}{t+1} \right) \right] \quad (1)$$

where $T$, $U$, $B$, and $N$ are the energy of the incident electron, the orbital kinetic energy, the binding energy, and the electron occupation number respectively, $t = T/B$, $u = U/B$, $S = 4\pi a_0^2 N(R/B)$, $a_0 = 0.529 \times 10^{18}$ Å, $R = 13.6057$ eV, the dipole constant $Q$ is approximated with 1, and n is a value near 1 used for ions [22].

The above parameters are based on experimental data [22]. Further, we correct this velocity to get the local velocity in a similar way as it was done for the Auger and photoelectrons. Now we should fix the velocity and position of the kicked out electron. However, this cannot be done simply, because we have a three body problem, and the energy and momentum conservation do not determine unambiguously the velocity of the ion and the primary electron after scattering. Therefore we assume, that the scattering of the incident electron is in the plane determined by the velocity of the primary electron before scattering and the vector pointing from the nucleus to the primary electron.

At this point the M.C. sub-step is finished. The next sub-step is solving the equation of motion. First we calculate the resultant force for every particle. Starting from the forces, the new velocities and positions are calculated using the fourth order Runge-Kutta method.

At the end of this section we describe the clusters investigated in this study. As model systems we chose monatomic all carbon clusters. The atoms were held together by simple central forces only. We used the following potential function:

$$V(r) = V_C \left[ \left( \frac{\sigma}{r} \right)^6 - 1 \right] \left( \frac{\sigma}{r} \right)^6 \quad (2)$$

where the values of $V_C$ and $\sigma$ parameters are chosen to have the minimum of the potential at $r = 1.5$ Å with the depth of 3.5 eV. Starting atomic positions were simple cubic or face-centered cubic ordered, or the above but with randomized positions about the lattice sites (we used $\max(|\Delta a|/a) = 0.05$, where $\Delta a$ is the deviation from the ideal lattice site, while "$a$" is the lattice spacing). We found that the actual starting atomic configuration hardly alters the explosion dynamics, as far as the first neighbor distance is kept the same. Therefore in what follows we show the results of calculations on clusters with the simple cubic atomic order.

## 3 Results

Before we show statistics, distributions, energy spectra etc. we would like to outline what type of information we seek and how we estimate the precision of our predictions [23]. Our aim is to map the characteristic behavior of clusters as a function of the size of the cluster (number of particles) and the length of the X-ray pulse. In size we covered the range from 50–1500 atoms/cluster. The pulse widths are $FWHM = 10$ and 50 fs. The most important features what we are interested in are: the total number of stripped electrons, the spatial and energy distributions of atoms, ions, and electrons, and the number of stripped electrons in the beam.

To see the effect and the importance of different interactions governing the time evolution of the system, we did three types of calculations. In these we turned on different interactions step by step. In the first one (referring later as model I) there are photo effect, Auger process, and Coulomb interaction between ions. However, the photo and Auger electrons leave the system without any interaction (we repeated the calculation of Neutze et al. [7] for our model system). It is clear that in these calculations we make two errors: first we underestimate the number of stripped electrons, since the photo and Auger electrons do not kick out further electrons from the atoms and ions. Secondly the rate at which the charge state of the cluster as a whole increases, is overestimated. This comes from the fact, that the positive ions attract electrons, so that the slower Auger electrons are unable to escape. At later times (i.e. for large charge state of the cluster, $Q > 10^4 e$) even the faster photoelectrons are significantly slowed down decreasing the temporary net charge of the cluster.

The underestimate in the number of stripped electrons means that the radiation damage is larger in reality than in the calculation of Neutze et al. [7]. However, this damage means a change in the charge state of the atoms and it does not necessary followed by a change in the position of atoms. Actually we expect slower increase of the positional disorder than predicted in [7] because of the overestimated total charge. In a real system a slower increase of the charge would lead to a milder Coulomb explosion.

In the second type of calculations (model II) we have the same interactions as in the first one, however, not only the ions but also the photo and Auger electrons interact by the Coulomb interaction. With this modification we correct for the above-mentioned overestimate. However, the total number of ionizations, which is important from the point of view of plasma dynamics, stays much behind the reality.

Therefore, in the third type of calculation (model III) we introduced inelastic electron-atom and electron-ion scattering in addition to the effects taken into account earlier. That results in the appearance of secondary electrons. However, in this case the number of stripped electrons is overestimated. This comes from the fact that in the classical equation of motion, atomic and ionic orbits are not quantized. Therefore a classical electron (stripped electron in our calculations) can drop very deep into the potential well of an ion, meanwhile the secondary electron takes the excess energy in the form of kinetic energy. This results in more stripped electrons, as we would have in reality. In order to compensate for this effect we did not allow negative binding energies between the two electrons participating in the process and their nearest neighbor ion. However, even with this adjustment a slight overestimate is expected for the number of stripped electrons, because electronic relaxation, recombination is not taken into account. They were left out because according to experiments [24,25] and theoretical estimates [17], these processes have very small probabilities on the time scale we are interested in.

The results we present are based on hundreds of calculations. Beside doing calculations for the different models and various cluster sizes, we also followed several independent explosions with the same parameters except using different series of random numbers. This way we could check the sensitivity of parameters to the stochastic nature of the processes. We found that the statistical uncertainty was about 5% for the 50-atom clusters and this fluctuation significantly decreased for larger clusters. The various parameters shown in the following figures are the result of averages of independent explosions. It is clear that we cannot show all the curves and real space distributions. Therefore, first we show typical results of one model calculation (Figs. 2 and 3) and explain the main features of these figures. Then in the next part, the different types of calculations will be compared and at the end the dynamics of the Coulomb explosion will be given for various cluster sizes and pulse lengths based on the most realistic model.

We have chosen for demonstration a 1500-carbon atom cluster. The atoms are arranged in a simple cubic lattice with lattice spacing of $a = 1.5$ Å and the starting atomic positions randomized about the regular lattice sites as described earlier. The pulse length is 50 fs and $5 \times 10^{12}$ photons are in a pulse. According to the categorization given earlier, the calculation is in the third category (all interactions are included). In Figure 2a we show the number of different type of particles as a function of time. Since we do classical calculations, we can flag electrons by their origin. That allows us to distinguish Auger, photo and secondary electrons. The curve labeled stripped electrons in the beam needs further explanation. It is calculated by counting the number of electrons in the volume of a 1000 Å diameter cylinder with its axis coinciding with the X-ray beam. The significance of this curve is that it allows to estimate the number of inelastically scattered photons of the incident beam. All numbers are normalized by the total number of electrons present in the sample at zero time. In Figures 2b, 2c and 2d we show the time evolution of the spatial distribution of stripped electrons, ions and the total charge respectively. The horizontal axis corresponds to the real space distance from the center of mass. The vertical axis denotes the time. The colors show the number of electrons in a 1 Å thick spherical shell with a radius corresponding to the values on the horizontal axis. In Figure 3 the cluster in real space is shown as if it were photographed at different times. At this point we do not want

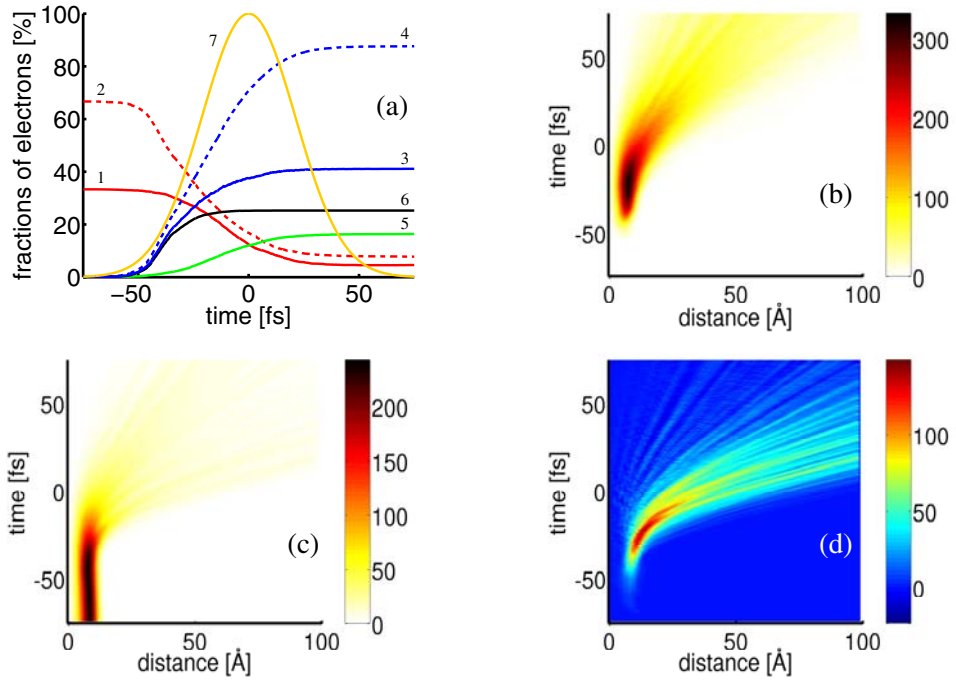


**Fig. 2.** General properties of an exploding atom-cluster in an X-ray pulse. The figures are for a 1500-carbon atom cluster in a 50 fs pulse. (a) Number of different types of electrons vs. time (curves: solid red (1) = K, dashed red (2) = L, solid blue (3) = stripped in the beam, dashed blue (4) = all stripped, green (5) = Auger, black (6) = secondary electrons, and yellow (7) = intensity of the beam). In (b), (c), and (d) the radial distribution (number of particles in a 1 Å thick spherical shell with radius $r$) of electrons, atoms/ions, and the total charge are shown respectively. Note that the middle of the pulse is at $t = 0$ fs. We use this convention for the time in all figures [a color version of Figure 2 is available in electronic form at `http://www.edpsciences.org`].

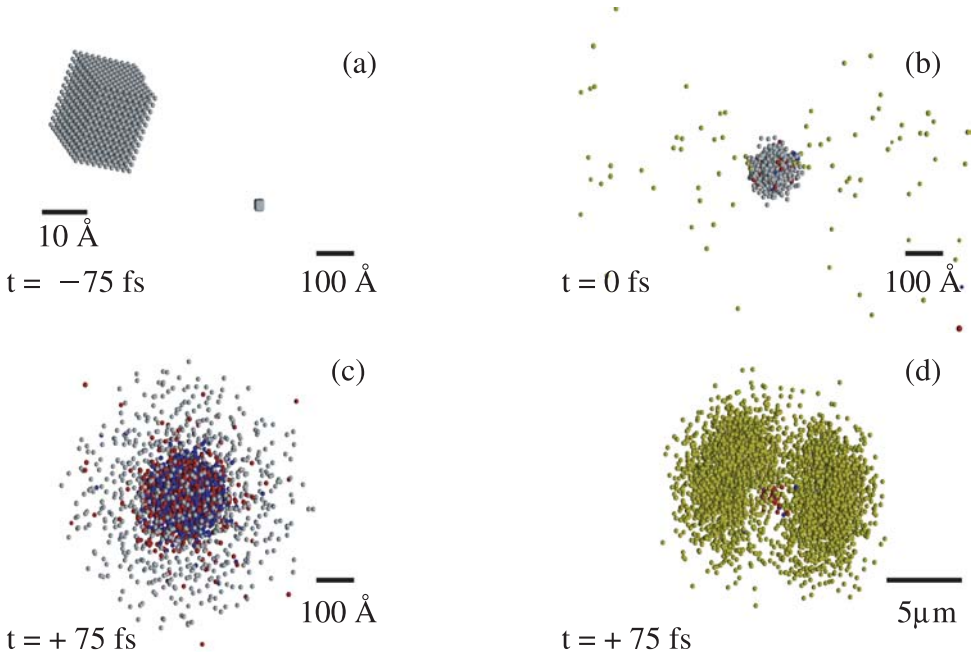


**Fig. 3.** An exploding 1500-atom cluster in real space at different times. The spheres with color gray, light green, red, and blue symbolize the atoms, photo-, auger-, and secondary-electrons, respectively. At the end of the pulse the radius of the cluster is about 15 times larger than it was originally (not including the photoelectrons). For better visualization we show the initial configuration of the cluster enlarged on the upper left part of (a). We used opposite zooming on (d) in order to show the photoelectrons escaped far away from the cluster. Mostly Auger and secondary electrons concentrate at the center (c), whereas photoelectrons are leaving the system forming a butterfly-shaped cloud (d), reflecting the anisotropy of the photoeffect in the linearly polarized X-ray [a color version of Figure 3 is available in electronic form at `http://www.edpsciences.org`].

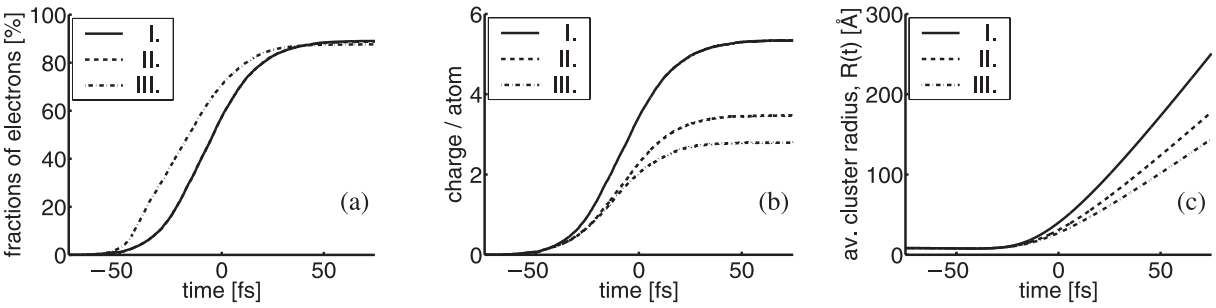


**Fig. 4.** The time evolution of the number of stripped electrons, the charge of the cluster/atom, and the average radius of the cluster are shown in (a), (b), and (c), respectively, for an exploding 1500-atom cluster. The three different curves denote the three types of model calculations: (I) with photo and Auger electron emission, without secondary ionizations, neglecting the presence of the non-bounded electrons; (II) including the photo and Auger electrons, but still excluding secondary ionizations; and (III) including secondary electron emission in addition to the interactions taken into account in I and II. Note that in (a) curve I and II exactly coincide.

to analyze Figures 2 and 3 in details but we point out a few features characteristic for all calculations: (i) atoms lose a significant number (∼70%) of their bound electrons within the first half of the X-ray pulse, (ii) photoelectrons leave the cluster shortly after their emission (but a significant number are in the beam), (iii) the butterfly shaped spatial distribution of photoelectrons reflects the direction of polarization of the incident beam. (iv) The cluster looses its nuclear topology very early during the pulse (well before half of the photons hit the sample).

After introducing the parameters, which characterize the explosion, we compare finer details predicted by different models (the three different types of calculations, introduced previously). We used the same parameters of the cluster and the pulse as in the experiment described in the previous paragraph. In Figures 4a, 4b, and 4c the number of stripped electrons, the average charge/atom (the degree of ionization), and the radius of the cluster ($R(t) = \sqrt{\frac{1}{N}\sum_i^N r_i(t)^2}$, where $N$ denotes the number of atoms in the cluster and $r$ their distance from the center of mass) are shown respectively. The figure clearly reflects those features discussed earlier in this section: the first type of calculation overestimates the increase of the charge (Fig. 4b), and it underestimates the ionization rate of atoms (Fig. 4a). Including Coulomb interaction for all charged particles (second type of calculation) we correct somewhat for the overestimate. This is best seen on the charge (Fig. 4b), but it also changes the dynamics of the Coulomb explosion, see the time dependence of $R(t)$ (Fig. 4c). We expect that the true behavior of the cluster is closest to the third type of calculations in which all interactions are taken into account. Therefore, in what follows we show the results of the third type of calculations only.

First we analyze the dynamics of the Coulomb explosion as a function of cluster size and pulse length. In Figures 5 and 6 we depicted the time dependence of the number of stripped electrons, the average charge/ion, and the normalized cluster size ($R_N(t) = R(t)/R(-\infty)$) for systems containing 50, 100, 200, 500, or 1500 particles. The pulse length was 10 fs and 50 fs respectively.

Let us start with the discussion of Figures 5a and 6a. There is a trend in the number of stripped electrons with the cluster size: the larger the cluster the faster the ionization. This can be explained by the secondary ionization, since for small clusters there is a larger chance for Auger and photoelectrons to leave the system without kicking out another electron. For first sight Figures 5b (Fig. 6b) and 5c (Fig. 6c) contradict Figure 5a (Fig. 6a), since the normalized size of the clusters and the average charge of the particles increase more slowly for larger clusters. The explanation of this effect is that photo and Auger electrons loose their energy on secondary ionization and their remaining kinetic energy is not enough to escape from the Coulomb attraction of the positive net charge of the cluster. These slow electrons shield the ion-ion repulsive Coulomb interaction, leading to slower Coulomb explosion of larger clusters.

Beside the time dependence of the number of "free" charges, their spatial distributions are also important characteristics of the explosion. In Figure 7 the radial charge distributions are shown for a 500 (Fig. 7a) and a 1500 (Fig. 7b) atom cluster, at the end of a pulse with $FWHM = 50$ fs. The behavior of the systems are similar in the case of a 10 fs pulse, therefore we do not show that figure separately. Note that there is a step in the charge distributions. We have an almost neutral plasma in the central part of the cluster and a highly charged shell around it. This charge distribution is formed from highly charged individual ions and electrons. To illustrate this, we depicted the charge distribution of ions independently. Note, that the degree of ionization is almost constant everywhere, it does not follow the net charge curve. Therefore the charge distribution is formed from highly charged ions and electrons and it is not the result of a high concentration of neutral atoms in the center part. In the following we discuss this peculiar charge distribution in more details. We show that the two spatially separated regions have different characteristics in the energy domain and that the border of these regions moves out continuously. We demonstrate this for large clusters, but one finds

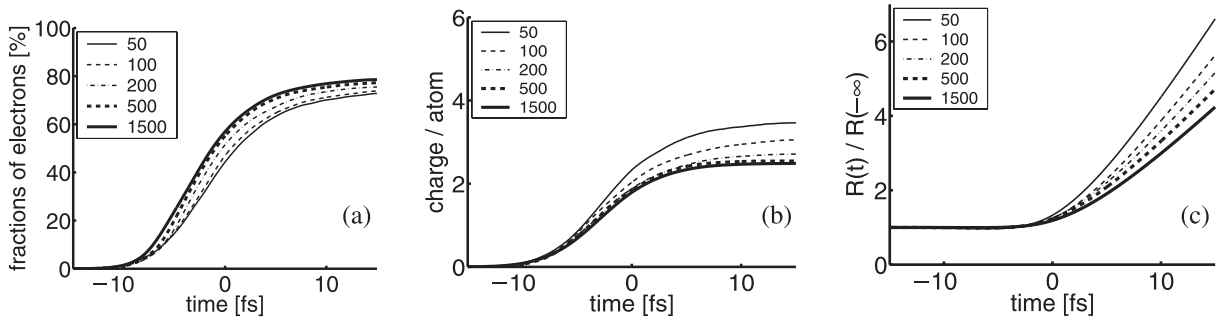


**Fig. 5.** Time evolution of the number of stripped electrons (a), the average total charge of the cluster per atom (b), and the radius of the cluster (normalized by the initial cluster radius) (c), in a 10 fs X-ray pulse. Various curve types correspond to clusters containing different number of atoms.

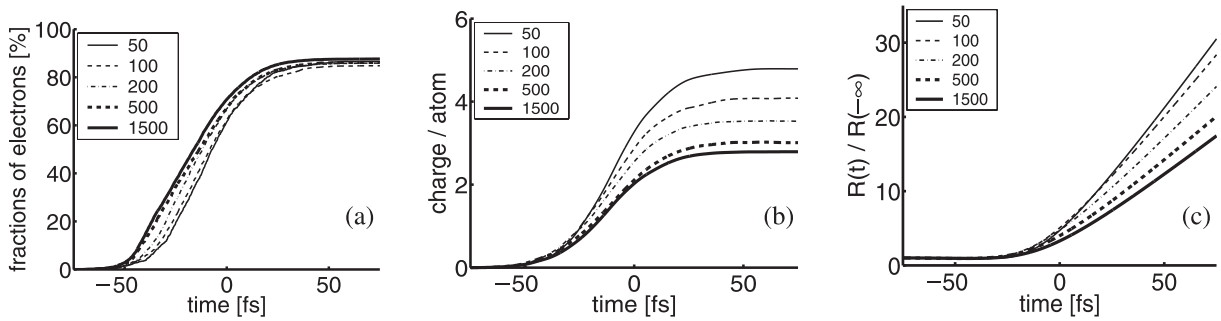


**Fig. 6.** Time evolution of the number of stripped electrons (a), the average total charge of the cluster per atom (b), and the radius of the cluster (normalized by the initial cluster radius) (c), in a 50 fs X-ray pulse. Various curve types correspond to clusters containing different number of atoms.

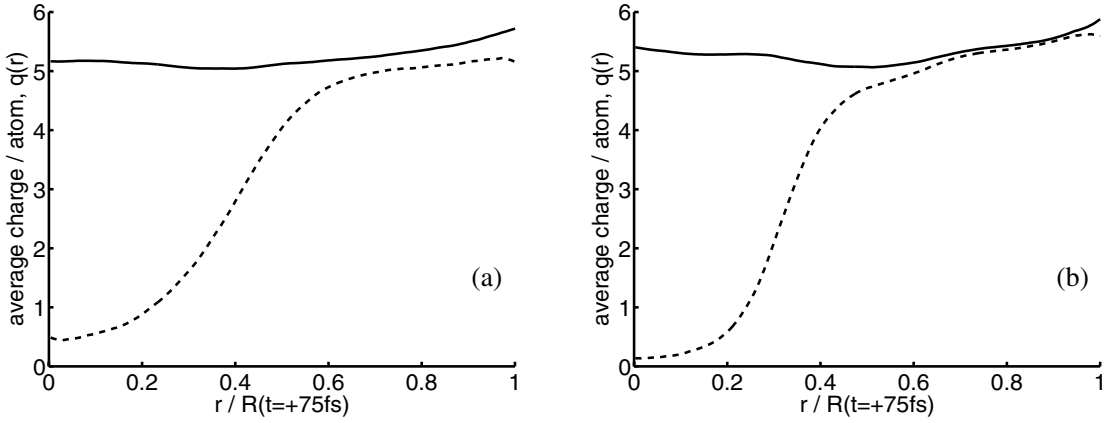


**Fig. 7.** Spatial distribution of the average ionic charge per atom (solid line) and the cluster-charge per atom (dashed line) in a cluster containing 500 (a) and 1500 (b) atoms, at the end of the pulse. Note that the distance from the center of mass is normalized for easy comparison.

similar behavior for smaller ones. We chose large systems because for small clusters (50–100 atoms) the definition of the border between the two regions is less precise. Figures 8a and 8b show the energy distributions of ions at various times during the pulse for a 500 and 1500 particle cluster, respectively. There are two characteristic features: (i) the energy scale is going up to the many keV range, and (ii) there are two regions in energy, a low energy peak and a long high energy tail. We defined a border between the two regions as the zero crossing of a straight line fitted to the steepest part of the energy distribution curve. Note that at the beginning of the pulse there is a time interval (or a minimum number of incident photons), for which the two regions cannot be defined, because there is not enough time and free electrons and ions to form these regions. In this particular case this interval extends to about −15 fs. We examined the characteristics of these regions separately. First we show the spatial distribution of the ions. In Figure 8c a typical curve of the number of ions as a function of the distance ($r$) from the center of mass is shown. The number of ions was calculated by counting the ions in 1 Å thick spherical shells with different

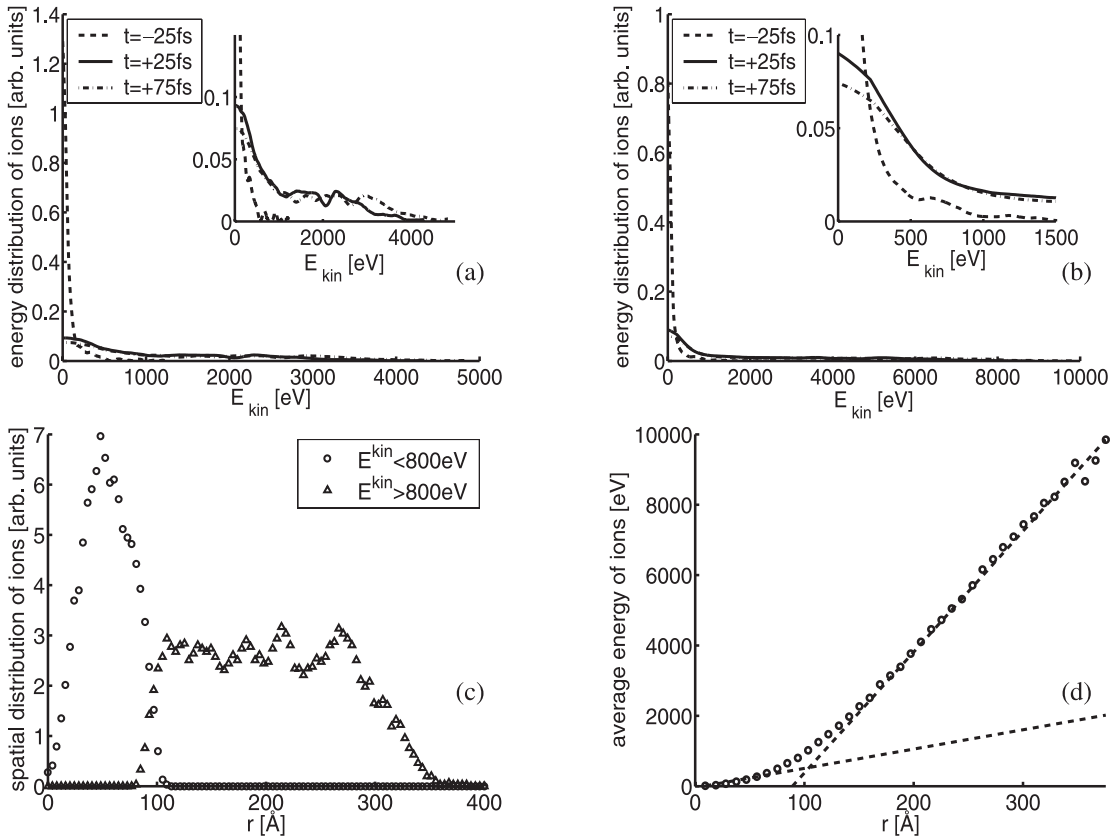


**Fig. 8.** Kinetic energy distributions of atoms at different times for 500 (a) and 1500 (b) atom clusters with enlarged energy regions in the insets. In (c) the radial distributions of atoms in the peak and in the tail are plotted using open circles and open triangles, respectively ($N = 1500$, $t = +75$ fs, $T_{pulse} = 50$ fs). In part (d) the radial distribution of the average kinetic energy is plotted. This curve can be described by two linear functions shown as dashed lines.

radiuses ($r$). The spatial distribution shows a similar shape as the energy distribution. It seems that the resemblance is not accidental, the separation in energy is connected to a separation in space: the low energy ions are close to the center, in the first peak; up to 80 Å. The ions in the high energy tail are further away, in the tail of the spatial distribution curve. This stronger correlation can be observed by plotting the average energy of ions as a function of the distance from the center of mass (Fig. 8d). A monotonic increase of the energy with the distance is observable. One can fit this curve by the sum of two linear functions. Their crossing coincides with the border of the almost neutral plasma and the highly charged outer shell, further emphasizing the distinction between the two regions. We can get an estimate for the speed of the Coulomb explosion from the motion of the border. We plotted the position of the border as a function of time in Figure 9. According to this, the border moves out with about 1.1 Å/fs velocity, which corresponds to ∼700 eV ion energy.

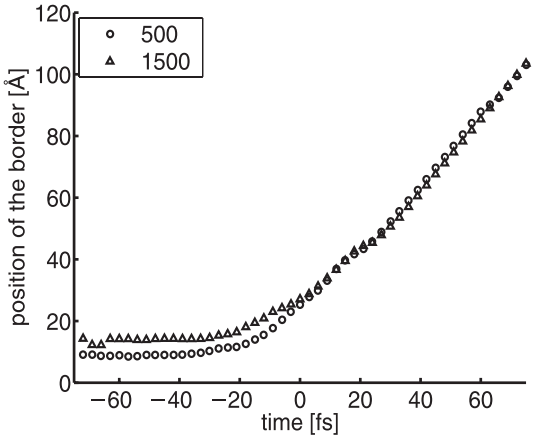


**Fig. 9.** Radius of the inner part of the cluster vs. time.

So far we examined the spatial and energy distribution of ions. In the next part we characterize the electrons. In Figures 10a–10c the energy distributions of electrons are shown for various cluster sizes (100, 500, and 1500) and at different times for pulse width of 50 fs. The combined effect of secondary ionization and expansion of the cluster is observable. As we approach the end of the pulse the energy distribution of electrons gets narrower, more electrons "condense" to small energies. This effect is more pronounced for larger systems, in which the secondary ionization is more effective. In order to estimate the effect of secondary ionization, we calculated the energy distribution for models without the secondary ionization. The result is shown in Figure 10d for a 50 fs pulse width and

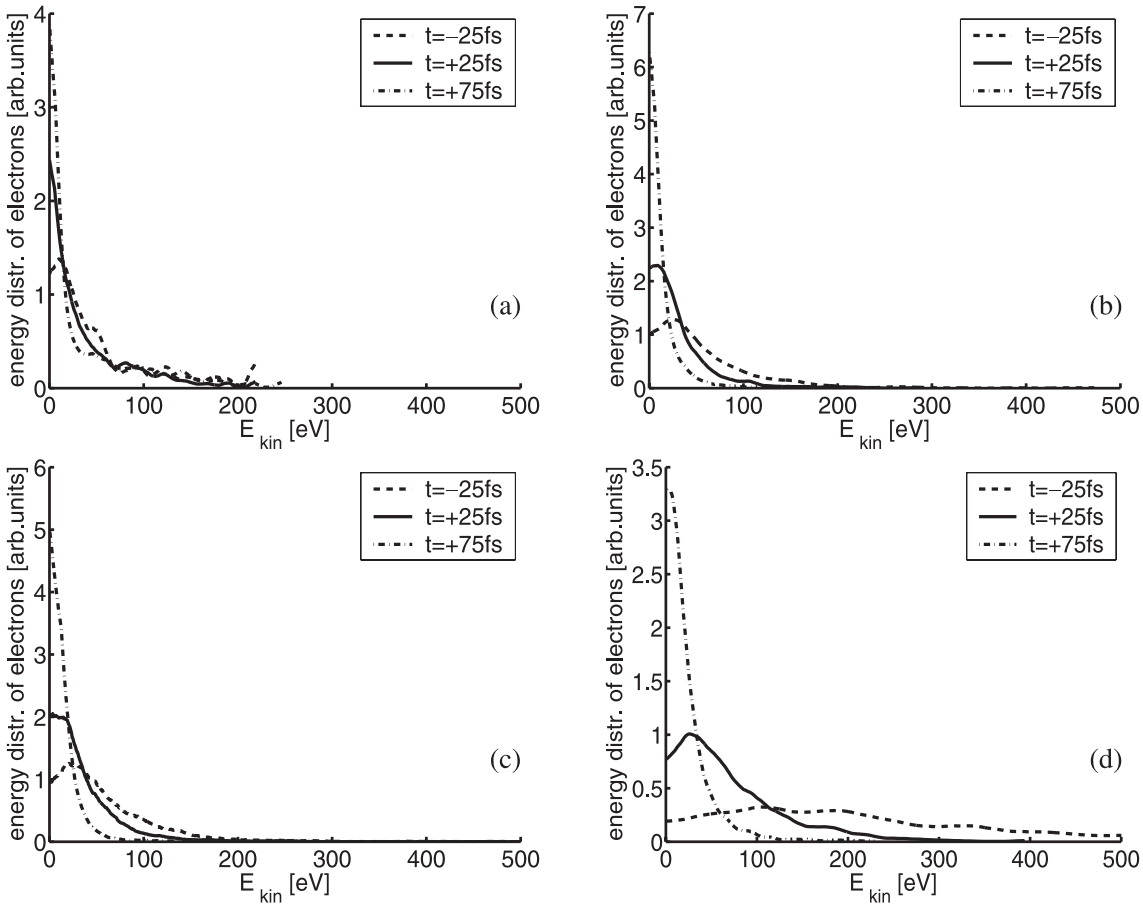


**Fig. 10.** Kinetic energy distributions of electrons inside the cluster at various times based in (a) 100-atom, (b) 500-atom, and (c) 1500-atom calculations in a $FWHM = 50$ fs pulse. For comparison in (d) we show the same distribution for a calculation excluding secondary ionizations ($N = 1500$, $FWHM = 50$ fs).

1500 particle system. Comparing this distribution to that of Figure 10c (the same system with secondary ionization), differences can be observed. The first general impression is that much less electrons are stripped. This is not surprising since we turned off an ionization process. The second feature is that the distributions get wider. This feature is more pronounced at the early time of the pulse.

Beside the above features of the energy distributions we can try to connect the energy to thermodynamic parameters. It is clear that the system is small and far from equilibrium, so thermodynamic parameters are hard to define. In spite of this, the knowledge of the relation between density and kinetic energy (temperature) might give a clue to the understanding of the governing processes. Therefore we depicted the average kinetic energy of ions and electrons inside the cluster as a function of the ion density, and the ion density as a function of the time, in Figures 11a, 11b, and 11c respectively. The $E(\rho)$ function of ions is characteristic for an exploding system, which we pump energy into. The energy has a rapid nonlinear increase at low densities. The electrons behave very differently, they are almost decoupled from the ions. Their energy is slightly, linearly decreasing with the density. A deviation from this behavior can be seen at very low and high densities. On the low density region there is a drop (see Fig. 11b) and at high densities there is a fluctuation in the energy. The drop is caused by the simultaneous effect of two factors: the decrease of energy deposition by the incident photon beam and the expansion of the cluster. The fluctuation is a result of the low number of stripped electrons and the very high energy of photoelectrons. High density appears at the early time of the pulse. However, this time the number of stripped electrons is very low, and mostly photoelectrons are present. If one or more of these high energy (∼10 keV) photoelectrons are in the cluster, where we calculate density and energy distribution, we get a high average. However, as the number of the secondary and Auger electrons increase, the weight of photoelectrons becomes small. In Figure 11c the time dependence of the ion density is shown. There is a narrow time interval (centered about −20 fs), where a large drop in the density takes place.

Before we finish the discussion of the results of our model calculations, we compare our findings to calculations published earlier. Unfortunately, there are not many works on this topic. The closest to our modeling is the calculation of Neutze et al. [7], which we have mentioned earlier in the paper. However, the aim of that work was

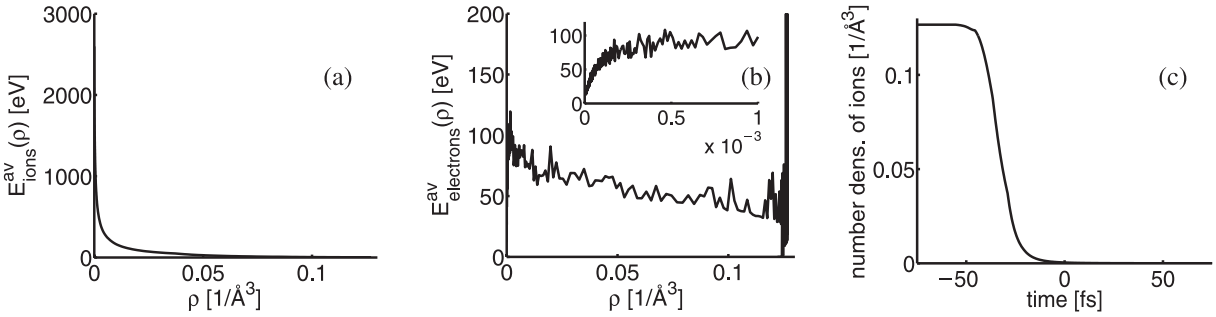


**Fig. 11.** Average kinetic energy of atoms (a) and electrons (b) inside the cluster vs. average atomic density $\rho$. Part (c) shows the time dependence of the average atomic density ($N = 1500$, $FWHM = 50$ fs).

not to give a detailed analysis of the plasma and its time evolution but to get an impression on the feasibility of single molecule imaging. Since in that paper there was no detailed data on the spatial, time and energy distributions of particles, we repeated that type of calculations with the same parameters we used in our modeling (these calculations correspond to the first type of modeling, according to our categorization introduced earlier). The basic differences between our modeling and the calculation performed in [7] is that we follow all stripped electrons (we do not remove them from the system), and all charged particles interact by Coulomb interaction. In addition to this, the electrons are also inelastically scattered by atoms and ions. These differences have two consequences: in one hand the ionization of atoms are faster, but at the same time the Coulomb explosion is moderated by the electron cloud formed by slow electrons. This results in a different explosion dynamics, and spatial charge and energy distributions. We find an almost neutral central core expanding by 1.1 Å/fs velocity, and a positively charged shell formed by fast highly ionized ions about this core. In Neutze's model this type of charge distribution does not develop.

Recently, there has been another publication on cluster dynamics at X-ray energies [26]. However, in this case the cluster size was small (13–55 argon atoms) compared to ours (50–1500 carbon atoms), and the photon energy much lower (350 eV) than in our modeling (10 keV). Therefore our findings differ from those of [26]. However, there are two similarities: ionization starts from inner shells, and the incident beam does not give appreciable velocity to charged particles, and therefore it causes negligible spatial oscillation.

The third type of works, which we can compare our calculations to are the works on the classical laser driven Coulomb explosion of small clusters. There have been extensive theoretical and experimental investigations in this area [27–31]. Comparing results we find substantial differences in every respects: spatial charge distribution, energy distribution and in time dependence. This is not surprising, since the underlying processes are different. The difference originates from the very long wavelength (hundreds of nm-s) of the incident beam compared to our case (0.1 nm). The consequences of the large wavelength are: at a given time the full cluster sees the same field; the direction of this field changes slowly compared to the time an electron moves about the cluster size; single photon energy is not enough to strip bound electrons. Since in the X-ray case we are in the opposite limits, the behavior of the cluster in the short X-ray and laser pulse is very different. This difference already manifests in the ionization process. While in the classical laser case the ionization proceeds by multiphoton ionization from outer shells and it is followed by impact ionization via the stripped fast electrons accelerated by the field. In the X-ray case the field of the incident beam does not play such an important role, since it does not accelerate stripped electrons to high velocities. The cause of this is that the field direction is changing so fast that charged particles can not gain appreciable velocity in this period. Therefore Auger and secondary electrons stay in the cluster, and as the cluster of ions expands the electrons condense to low energies. These electrons slow down the Coulomb explosion, especially in the inner core of the ion cluster. This very different explosion dynamics also reflects in the energy distribution of ions. In the X-ray case the typical ion energies are much lower. They are in the 10 keV range as compared to the hundreds of keV found in classical laser driven Coulomb explosions.

After finishing the characterization of the Coulomb explosion, a few words are appropriate about the time scale in which the validity of our model calculation is justified. A limit is given by the recombination processes, which we neglected. Recombination plays an important role if a large ratio of the electrons localize about ions with small energy. To see this, we counted how many electrons stay at an ion for long periods [32]. This is shown in Figures 12a and 12b for 10 and 50 fs pulse width. The result correlates very well with the energy distribution given in Figures 8, 10, and 11. As the energy of the particles and the density decreases, the temporary localization increases. However, even in the worst case, approximately 50% of the photons stay about 10 fs at a given site. Comparing this to typical recombination times (1000 fs), the probability of the recombination is small.

At last we would like to discuss shortly the consequences of our calculations on the single molecule imaging suggested by Neutze et al. [7]. First, we would like to point out that the assumption of neglecting the interaction of photo- and Auger electrons with the cluster is justified only for small clusters (<500 atoms).

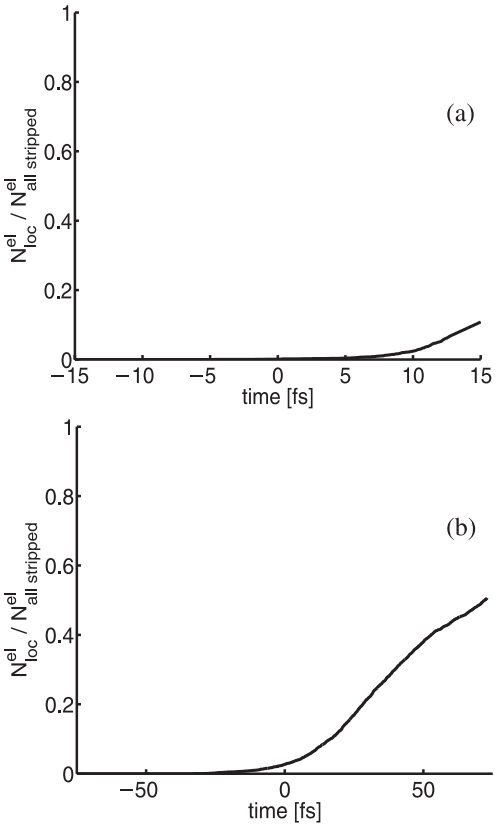


**Fig. 12.** Fraction of electrons, which are classically localized for a 1500 atom cluster in a 10 fs (a) and in a 50 fs (b) pulse are shown as a function of time [32].

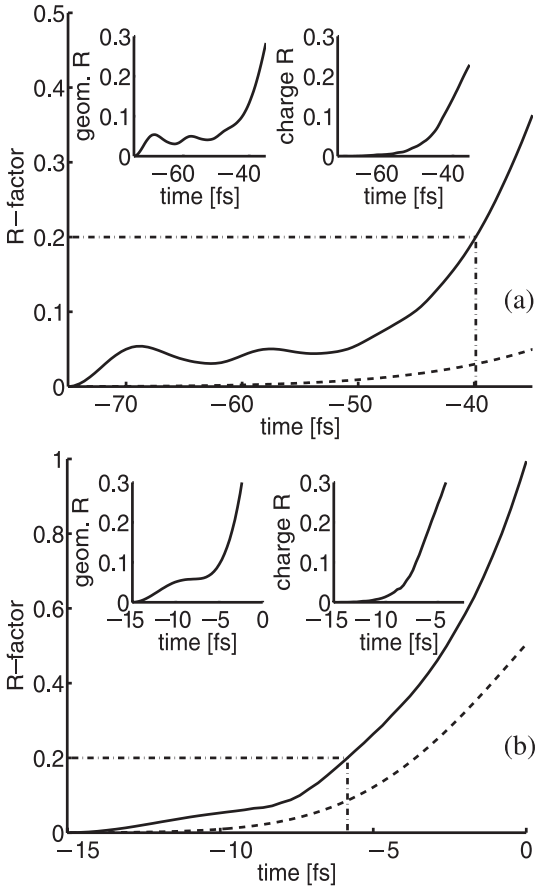


**Fig. 13.** $R$-factors calculated from the geometrical distortion (geom $R$) and from the changing of the average number of atomically bound electrons (charge $R$) for a 1500 atom cluster in a 50 fs (a) and in a 10 fs (b) pulse. The insets show the contribution of the geom $R$ and charge $R$ separately. The dashed line shows the integral number of photons.

As it is clear from Figure 4c the authors overestimated the speed of the Coulomb explosion. This would mean an even higher tolerance against radiation, and a better chance of successful imaging by a single pulse. However, it is not enough to have the nuclei at their proper positions, we must have electrons bound to the nuclei to scatter X-ray photons. As we can see from Figure 4a, the number of stripped electrons was underestimated in Neutze's calculations. This error increases with cluster size. To estimate the time available for imaging, we calculated the deviation of temporary atomic configuration from the original one (Fig. 13). We took into account two contributions: structural deviation (position changes, $\Delta r_i$) and ionization state (how many electrons remain on the atoms to scatter; changes in the atomic scattering factors $\Delta f_i$). Allowing 20% overall error we can measure up to $-40$ and $-6$ fs in the case of 50 and 10 fs pulses respectively, to get useful structural information. Since the pulse shape is Gaussian, it is not easy to visualize the meaning of these limits. A better characterization can be given by the integral number of photons incident on the sample within this period. We find that these are 3% and 10% of the total number of photons in the case of a 50 and a 10 fs pulse, respectively. In practice this means that we have to disable our detector during the major part of the pulse. A more detailed analysis on the structural studies of small single particles by hard X-ray free electron laser pulses will be given in a forthcoming paper.

## 4 Conclusions

In this paper we gave a picture of the Coulomb explosion of a small cluster of atoms initiated by a hard X-ray pulse. In the calculations we covered a wide range of cluster size from 50 to 1500 particles/cluster for short (10 fs) and for long (50 fs) pulses. We showed that the dynamics of the explosion is different from that of the laser driven Coulomb explosion. The cause of this is twofold: (i) ionization of atoms starts from the deepest core levels in contrast to the laser case, where it starts from the weakly bound outer shells. (ii) The high frequency of the electromagnetic field in the X-ray case does not allow charged particles to gain appreciable velocity along the field direction. These lead to the following picture: most of the electrons kicked out by the primary photoeffect have high enough kinetic energy to leave the close environment of the cluster well within the time width of the X-ray pulse.

This results in a positively charged cluster. However, this primary ionization is enhanced by the Auger process and by the inelastic electron-atom and electron-ion collisions. Electrons produced this way do not have enough energy to leave the cluster immediately, a peculiar charge distribution is created from highly charged ions and electrons. This distribution is inhomogeneous; a closely neutral core is surrounded by a positive shell. At the end of the pulse three typical energy distributions can be distinguished: electrons in the inner almost neutral core condense at low energies, most of the ions in this inner part have also low energies, the remaining ions are in the positively charged shell having a closely constant energy distribution at the high energy side.

Beside the characterization of the Coulomb explosion, we also gave an estimate for the useful time for structural imaging of small clusters. We found that about the 3% and 10% of the total number of photons in a pulse can be efficiently used for structural imaging from a 50 and 10 fs pulse, respectively.

The work reported here was supported by the EU Centre of Excellence program, OTKA T029931, T043237, and the EU BIO-4CT98-0377 grant. We thank Janos Hajdu, Abraham Szöke, and Beata Ziaja for the illuminating discussions.

## References

1. G. Materlik, T. Tschentscher, *LCLS and TESLA feasibility reports, The X-ray free electron laser*, TESLA Technical Designe Report (2001)
2. J. Arthur, Rev. Sci. Instrum. **73**, 1393 (2002)
3. Z.Y. Chen, C.D. Cogley, J.H. Hendricks, B.D. May, A.W. Castleman, J. Chem. Phys. **93**, 3215 (1990)
4. T. Ditmire, Nature **386**, 54 (1997)
5. Y.L. Shao, T. Ditmire, J.W.G. Tisch, E. Springate, J.P. Marangos, M.H.R. Hutchinson, Phys. Rev. Lett. **77**, 3343 (1996)
6. T. Ditmire, J. Zweiback, V.P. Yanovsky, T.E. Cowan, G. Hays, K.B. Wharton, Nature **398**, 489 (1999)
7. R. Neutze, R. Wouts, D. van der Spoel, E. Weckert, J. Hajdu, Nature **406**, 752 (2000)
8. K.S. Trainor, J. Appl. Phys. **54**, 2372 (1983)
9. S.H. Glenzer, K.B. Fournier, C. Decker, B.A. Hammel, R.W. Lee, L. Lours, B.J. MacGowan, A.L. Osterheld, Phys. Rev. E **62**, 2728 (2000)
10. B. Ziaja, D. van der Spoel, A. Szöke, J. Hajdu, Phys. Rev. B **64**, 214104 (2001)
11. B. Ziaja, A. Szöke, D. van der Spoel, J. Hajdu, Phys. Rev. B **66**, (2002) 024116
12. In half period of the X-ray frequencies an electron changes its velocity by about $v = 3 \times 10^6$ m/s (corresponding to $E_{kin} = 30$ eV) and its position by $s = 0.002$ Å.
13. The value of $r_0$ was 0.25 Å
14. W. Heitler, *The Quantum Theory of Radiation* (Clarendon Press, Oxford, 1954)
15. L.V. Azaroff, *X-Ray Specroscopy* (McGraw-Hill Inc, USA, 1974)
16. M.O. Krause, J.H. Oliver, J. Phys. Chem. Ref. Data **8**, 329 (1979)
17. L.D. Landau, E.M. Lifschitz, *Quantum Mechanics (Non-Relativistic Theory)* 3rd edn. (Pergamon Press, Oxford, England, 1977)
18. S. Tanuma, C.J. Powell, D.R. Penn, Surf. Interf. Anal. **11**, 577 (1988)
19. S. Tanuma, C.J. Powell, D.R. Penn, Surf. Interf. Anal. **17**, 911 (1991)
20. J.C. Ashley, J. Electr. Spectrosc. Relat. Phenom. **50**, 323 (1990)
21. J.C. Ashley, J. Appl. Phys. **69**, 674 (1991)
22. Y.K. Kim, M.E. Rudd, Phys. Rev. A **50**, 3954 (1994)
23. On precision we mean the systematic errors caused by the approximations (what processes are taken into account) used by the different models. Turning on and off a process we can get an estimate for the importance of that process
24. S.N. Nahar, A.K. Pradhan, Astrophys. J. Suppl. **111**, 339 (1997)
25. U.I. Safronova, T. Kato, J. Phys. B **31**, 2501 (1998)
26. U. Saalmann, J.-M. Rost, Phys. Rev. Lett. **89**, 143401 (2002)
27. C. Rose-Petruck, K.J. Schafer, K.R. Wilson, C.P.J. Barty, Phys. Rev. A **55**, 1182 (1997)
28. T. Ditmire, Phys. Rev. A **57**, R4094 (1998)
29. I. Last, J. Jortner, Phys. Rev. A **60**, 2215 (1999)
30. I. Last, J. Jortner, Phys. Rev. A **62**, 013201 (2000)
31. V.P. Krainova, M.B. Smirnovb, Phys. Rep. **370**, 237 (2001)
32. The number of the localized electrons was determined by going backwards in the calculations (so starting from the end), and counting those electrons, which stayed longer than 1, 2, etc. fs in the vicinity of the same atom. Note that this way we can speak about localization only within the time frame of our calculation, we call this temporary localization